Thermal X-Ray Emission and Cooling of Solid Quark Stars

M. Yu* and R. X. Xu

School of Physics and State Key Laboratory of Nuclear Physics and Technology, Peking University, Beijing 100871, China

8 October 2009

ABSTRACT

We present a theoretical model for the thermal X-ray emission properties and cooling behaviors of isolated pulsars. It is assumed that pulsars are solid quark stars. Using Debye elastic medium theory, we calculate the heat capacity of such a quark star and show that the residual thermal energy cannot sustain the observed thermal X-ray luminosities seen in typical isolated X-ray pulsars. We conclude that another heating mechanism must be in operation if the pulsar is in fact a solid quark star. Two possible alternative heating mechanisms are explored. First, for pulsars with little magnetospheric activity, accretion from the interstellar medium or from material in the associated supernova remnant may power the observed thermal emission. A disk-accretion rate $\dot{M} \sim$ 1 % of the Eddington rate, with an accretion onto the stellar surface at a rate of $\sim 0.1\% \dot{M}$, could explain the observed emission properties of dim isolated neutron stars as well as central compact objects. Second, for pulsars with significant magnetospheric activity, the spindown of the pulsar itself may be providing the source of thermal energy via the reversing plasma current flow. A phenomenological study between pulsars' bolometric X-ray luminosities and their spin energy loss rates presents the probable existence of a 1/2-law or a linear law, i.e. $L_{\rm bol}^{\infty} \propto \dot{E}^{1/2}$ or $L_{\rm bol}^{\infty} \propto \dot{E}$. This result together with the thermal properties of solid quark stars allows us to calculate the thermal evolution of such stars. Cooling curves are calculated and compared with the thermal emission properties measured from 17 active X-ray pulsars. It is shown that the observed properties of these sources are consistent with the solid quark star pulsar model.

Key words: dense matter - stars: neutron - pulsars: general

1 INTRODUCTION

The study of cold quark matter phases has been a hot topic of research in recent years. In an astrophysical context, quark matter may be used to explain the measureable properties of pulsar-like compact stars.

It has recently been proposed that realistic quark matter could exist in a solid state (Xu 2003; Horvath 2005; Owen 2005; Mannarelli, Rajagopal & Sharma 2007), either as a super-solid or as a normal solid (Xu 2009). The basic conjecture of normal solid quark matter is that de-confined quarks tend to form quark-clusters when the temperature and density are relatively low. Below some critical temperature, these clusters could be in periodic lattices immersed in a degenerate, extremely relativistic, electron gas. Note that even though quark matter is usually described as weakly coupled, the interaction between quarks and gluons in a quark-gluon plasma is still very strong (Shuryak 2009). It

is this strong coupling that could cause the quarks to cluster and form a solid-like material.

In this paper, we argue that comtemporary observations of thermal X-ray emitting pulsars are consistent with the assumption that these sources are in fact Solid Quark Stars (SQSs). As it turns out, the heat capacity of solid quark matter can be easily estimated using Debye elastic medium theory. This is done in section §2. It is also shown that the internal energy of a SQS would be radiated almost instantaneously after its birth. Hence, if pulsars are SQSs, the observed thermal X-ray radiation must be powered by some other sources of energy. Two possible energy sources are proposed. The observing consequences of these models are discussed in §3. Our conclusion are discussed in §4.

2 THE MODEL

2.1 Cooling stages of a quark star

The cooling process of a quark star can be quite complicated to model when starting from the birth of the star. Theo-

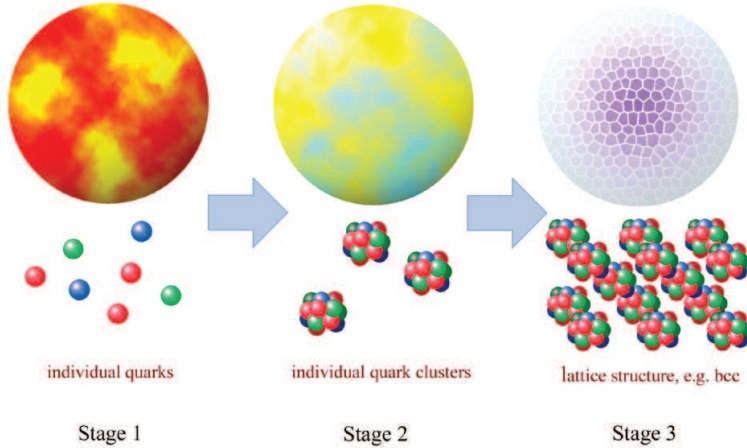* E-mail: vela.yumeng@gmail.com

Figure 1. Possible cooling stages of a quark star. *Stage 1*: individual quark phase. The temperature is high (> 10 MeV) when the star is born, and the state of the star could be the fluid of individual quarks. *Stage 2*: individual quark cluster phase. As the temperature decreases, individual quarks tend to form quark clusters because of the strong coupling between them. The state of the star could then be the fluid of quark clusters. *Stage 3*: solid quark star phase. As the temperature drops to the melting temperature, the fluid of quark clusters tend to solidify to form periodic lattice structure, such as bcc structure.

retical uncertainties make it difficult to predict the exact temperatures where phase transitions occur. For illustrative purposes, we present the following scenario where a SQS's cooling takes place in approximately three stages (See Fig. 1). The first stage occurs just after the birth of the quark star if its initial temperature is much higher than $\sim 10^{11}$ K (10 MeV). The emission of neutrinos and photons will lead to fast cooling. Hence, the star quickly enters the second stage where de-confined quarks begin to form quark clusters. As the temperature drops further, the fluid solidifies and the star is said to enter the third cooling stage. Here, quark clusters form periodic lattice structures (e.g. the bcc structure).

It is uncertain exactly how long the star will spend in each phase, or even if it will ever enter all three states. If the initial temperature is only just around 10^{11} K or lower, Stage 1 may be short lived or even non-existent. The quark-gluon plasma could be strongly coupled at birth and quark-clusters could be present immediately after formation. It is even possible that the melting temperature of solid quark matter could be 10^{11} K or higher. Hence, a SQS would enter Stage 3 immediately.

The mechanisms for the emission of thermal photons for each specific stage could be quite different. Hot quark stars (in Stages 1 or 2) could be a good radiator for thermal equilibrium photons with energies more than ~ 20 MeV (Alcock, Farhi & Olinto 1986). Meanwhile, the intense release of thermal energy could stimulate the generation and radiation of electron-positron pairs from the hot bare quark surfaces; nonthermal photons generated by electron-electron bremsstrahlung processes could also be an emitting component though the amount could be small (Usov 2001). When the stars cool down and become solidified (in Stage 3), thermal equilibrium photons (usually soft X-ray) could also be emitted from bare SQSs' surfaces as free electrons transit in the levels of the energy bands of solid quark matter (Xu 2003). The electron-phonon interaction as well as the

interaction between electrons themselves could result in a metal-like spectrum. Zhang, Xu & Zhang (2004) have analyzed this spectrum phenomenologically, but they did not conclude that there are significant differences between the metal-like spectrum and black body spectrum. Hence, black body thermal spectrum could be a good approximation for SQSs.

This work concentrates its attention on the late third stage with surface temperature varies between $\sim 10^7$ and $\sim 10^5$ K, which is the range of thermal components of isolated pulsars that telescopes have detected. The neutrino cooling could be negligible for a SQS in the late third stage, since the temperature then is low enough and the photon luminosity may dominate (Yakovlev & Haensel 2003). This situation is quite different from a normal neutron star, which is surrounded by a nearly adiabatic blanket (i.e., the crust; Gudmundsson, Pethick & Epstein 1983). Hence, in this stage, the stars cool down by losing thermal photons, and the sources of the energy that enable the thermal emission are firstly the residual thermal energy of the stars and secondly the energy input caused by the processes of stellar heating. The energy relation could then be described as

$$-\frac{\mathrm{d}U}{\mathrm{d}t} + L_{\mathrm{SH}} = L_{\mathrm{bol}}, \tag{1}$$

where L_{bol} is the stellar bolometric X-ray luminosity, $-\mathrm{d}U/\mathrm{d}t$ is the release rate of the stellar residual thermal energy, and L_{SH} is the luminosity of stellar heating.

2.2   Residual thermal energy of a SQS

Provided that the volume of a SQS is a constant, then the stellar residual thermal energy U_{SQS} could only be the function of the star's temperature T_{s},

$$U_{\mathrm{SQS}}(T_{\mathrm{s}}) = \int C_v \mathrm{d}T_{\mathrm{s}}, \tag{2}$$

where T_s is the value in the star's local reference frame, and C_v is the heat capacity of the star. Following Debye elastic medium theory, the characteristic of the heat capacity of solid quark matter could be evaluated by Debye temperature,

$$\theta_D = \hbar\omega_D/k_B, \tag{3}$$

where $\hbar$ is reduced Planck constant, and k_B is Boltzmann constant. ω_D is Debye cut-off frequency (i.e. the maximum frequency of the wave that could propagate in a medium), which equals Debye wave number $k_D = (6\pi^2 n_c)^{1/3}$ (n_c is the number density of classical particles, or quark clusters for solid quark matter especially) multiply the average sound speed in the medium, i.e. $\omega_D = k_D \bar{c}_s$. For a SQS, the average sound speed could be the light speed approximately. A linear equation of state, extended to be used for a quark star, notes that the pressure $p \sim \rho c^2$, where ρ is the mass density of a quark star, and c is the speed of light, so an estimate could be $\bar{c}_s = \sqrt{dp/d\rho} \sim \sqrt{p/\rho} \sim \sqrt{\rho c^2/\rho} = c$. $n_c = 3\epsilon n_0/A$, where ϵ denotes the baryon number density of solid quark matter in the unit of n_0. n_0 is the baryon number density of normal nuclear matter and equals 0.17 fm^{-3}. We consider $\epsilon = 3 - 5$ could be the representative values for a SQS. Noting that in the following calculation in this paper, we will adopt $\epsilon = 3$ as a typical value, since the variation of ϵ between 3-5 could not lead to the magnitudes of the results varying in orders. A is the number of valence quarks in a quark cluster. We may expect that A could be in the order of 10, since $A = 18$ if quark-α-like clusters are formed (Michel 1988; Xu 2003), and A could even be conjectured to be in the order of $\geqslant 10^2$. Debye temperature, θ_D, of a SQS could then be of order $\sim 10^{12}$ K, even higher than the temperature when a SQS is born. Hence, the heat capacity in the low-temperature limit, or the temperature-cube law, is applicable for the third stage, i.e.

$$c_v = \frac{12\pi^4}{5} k_B \left(\frac{T_s}{\theta_D}\right)^3, \tag{4}$$

where c_v is the heat capacity per classical particle (or quark cluster when refers to solid quark matter)(Vonsovsky & Katsnelson 1989), and $C_v = N c_v$, where N is the total number of clusters in a star.

By referring to equation (2), the residual thermal energy for a 1.4M$_\odot$-SQS could thus be $U_{SQS} \sim 10^4 T_s^4$ ergs, while the corresponding value for such a typical neutron star is $U_{NS} \sim 10^{30} T_s^2$ ergs (Yakovlev & Pethick 2004). Therefore, the residual thermal energy of a SQS will always be much less than that of a normal neutron star; even when the temperature is as high as $\sim 10^{11}$ K, the residual thermal energy of a SQS is only one ten thousandth of that of a neutron star. So if the cooling process of a 1.4M$_\odot$-SQS is only powered by its residual thermal energy, i.e.

$$-C_v \frac{dT_s}{dt} = 4\pi R^2 \sigma T_s^4 + \frac{4}{3}\pi R^3 10^{24} T_{s,9}^6 \tag{5}$$

(R is the local stellar radius, σ is Stefan-Boltzmann constant), then its cooling time scale from 10^{11} K to an extremely low final temperature 1 K is only ~ 0.2 s. Noting that as a result of the concerning of the high initial temperature here, neutrino luminosity for the SQS is also considered as the second term in the right side of the equal sign of equation (5) (Yakovlev & Haensel 2003). This could be the

intrinsic distinction for SQSs from neutron stars. Neutron stars' cooling is mainly residual thermal energy powered, while SQSs' thermal X-ray emission and cooling processes could however be sustained by heating processes.

2.3 Stellar heating

Heating processes may play a significant role in the thermal evolution or realizing the visibility of pulsars in the soft X-ray band, and pulsars with different magnetospheric properties may be undergoing different heating mechanisms.

2.3.1 Spin origin

Luminous nonthermal radiation and bright pulsar wind nebulae (PWNe), these observing manifestations may imply an active magnetosphere and strong star wind or relativistic particle flow could be ejecting from the poles of such a pulsar. A certain amount of backflow of such plasma induce the stellar heating, or an energy input could take place at the polar caps but disperse to the bulk of the star (Cheng & Ruderman 1977; Arons 1981; Zhang & Harding 2000; Wang et al. 1998). The heat flow, H, could thus be

$$H \sim \frac{L_{SH} - 4\pi r_p^2 \sigma T_p^4}{\pi r_p^2} \sim \kappa \frac{T_p - T_s}{R}, \tag{6}$$

where σ is Stefan-Boltzmann constant, $r_p \approx R\sqrt{\Omega R/c}$ and T_p are the radius and the surface temperature of polar caps in the local reference frame respectively, R is the local stellar radius. To the simplicity, we adopt the one dimensional approximation for the gradient of temperature, i.e. $\nabla T \sim (T_p - T_s)/R$. L_{SH}, the luminosity of the return-current stellar heating, could be a function of the spin energy loss rate $\dot{E}$, and could generally be in the form of a power law. However, a phenomenological study on the bolometric luminosity and $\dot{E}$ reveals that the power index could be 1/2 or 1, i.e. $L_{SH} = C\dot{E}^{1/2}$ or $L_{SH} = \eta\dot{E}$ (see Appendix A).

The metal-like interior of a SQS could imply that its thermal conductivity κ could be the sum of partial components of phonons, electrons, and static impurities, or

$$\kappa = \kappa_p + \kappa_e + \kappa_{imp}, \tag{7}$$

where the subscripts 'p', 'e', and 'imp' denote the partial components mentioned above, respectively. The electron thermal conductivity, κ_e, could be the dominant component for the solid metal (Flowers & Itoh 1981). So phonons' contribution, κ_p, could be neglected, and, as a preliminary model, we omit the partial component of static impurities. The electron thermal conductivity could be written as

$$\frac{1}{\kappa_e} = \frac{1}{\kappa_{ee}} + \frac{1}{\kappa_{pe}}, \tag{8}$$

where κ_{ee} is the partial component contributed by the collision between electrons, and κ_{pe} is the one contributed by the collision between phonons and electrons. For their analytic formulae, we refer to Flowers & Itoh (1981) with assuming that the results remain hold for SQSs.

2.3.2 Accretion origin

Some pulsars, showing steady long-term soft X-ray fluxes, being inert in nonthermal emission, lacking the proves on the

existences of the associated PWNe, (and sometimes) owning excesses of X-ray luminosities relative to the spin energy loss rates, could alternatively be inactive pulsar candidates. Due to their little magnetospheric manifestations, SQSs will not suggest the thermal X-ray radiation of these sources is of spin origin.

One possible way to understand the origin of the energy is the accretion in the *propeller* regime. In this regime, a shell of atmosphere of matter may form surrounding the star. Matter closing to the inner boundary of the shell may interact directly with the rotating stellar magnetosphere, as a result of which most of the matter will be expelled outward (Lipunov 1992). Nevertheless, a certain fraction of the accreting material, described by the accretion efficiency $\eta_{\rm acc}$, may diffuse starward and fall onto the surface of the star finally. In the propeller regime, the star's magnetosphere radius or Alfvén radius $r_{\rm m}$ could be on one hand larger than its corotation radius $r_{\rm co}$, but is on the other hand somewhat smaller than the light cylinder radius $r_{\rm L}$, i.e.

$$r_{\rm co} = (\frac{GM}{4\pi^2})^{1/3} P^{2/3} \lesssim r_{\rm m} = (\frac{R^6 B_{\rm p}^2}{\dot{M}\sqrt{2GM}})^{2/7} \lesssim r_{\rm L} = \frac{cP}{2\pi}, (9)$$

where G is the gravitational constant, M, R, and $B_{\rm p}$ are the stellar mass, radius, and the magnetic strength at the poles, respectively. The accretion rate $\dot{M}$ could be scaled by Eddington accretion rate $\dot{M}_{\rm Edd}$; so μ could denote the accretion rate in this unit, i.e. $\dot{M} = \mu\dot{M}_{\rm Edd}$. During the accretion of the material which could reach the stellar surface eventually, the energy of gravitation will be released. When the two-flavor baryonic matter impact upon the surface of a SQS, it will burn into the three-flavor strange quark matter phase, and the latent heat of $\Delta\varepsilon \sim 10$ MeV – ~ 100 MeV per baryon could be released in the phase transition (Madsen 1999). The luminosity of stellar heating in this situation could then be

$$L_{\rm SH} = \frac{GM \cdot \eta_{\rm acc} \cdot \dot{M}}{R} + \Delta\varepsilon \frac{\eta_{\rm acc} \cdot \dot{M}}{m_{\rm p}}, (10)$$

where $m_{\rm p}$ is the mass of a proton.

3   OBSERVATIONS VERSUS EXPECTATIONS

We concentrate on those X-ray sources, which demonstrate significant thermal emission, own ordinary magnetic fields 10^{11-13} G, own comparatively young ages 10^{3-6} yrs, and have spins of a few tens of milliseconds to a few seconds. We mainly refer to the collation made by Yakovlev et al. (2008) on cooling neutron stars, by Becker & Aschenbach (2002) on X-ray pulsars, by Haberl (2004) on X-ray dim isolated neutron stars (XDINs), and by Pavlov, Sanwal & Teter (2004) on central compact objects (CCOs). The sample exhibited in Table 1 thus comprises top 17 active pulsar candidates, 7 XDINs (No. 23-29) and 6 CCOs (No. 5 and 18-22). We note that the values of the surface temperatures adopted are determined by black body fits, according to the way that a SQS emits thermal photons. The XDINs and CCOs are considered to be magnetosphere-inactive pulsar candidates, since their quiescent manifestation on nonthermal radiation. CCOs, moreover, could only be seen in the soft X-ray band without the evidences on the existence of the associated PWNe. Additionally, we note that the emission of
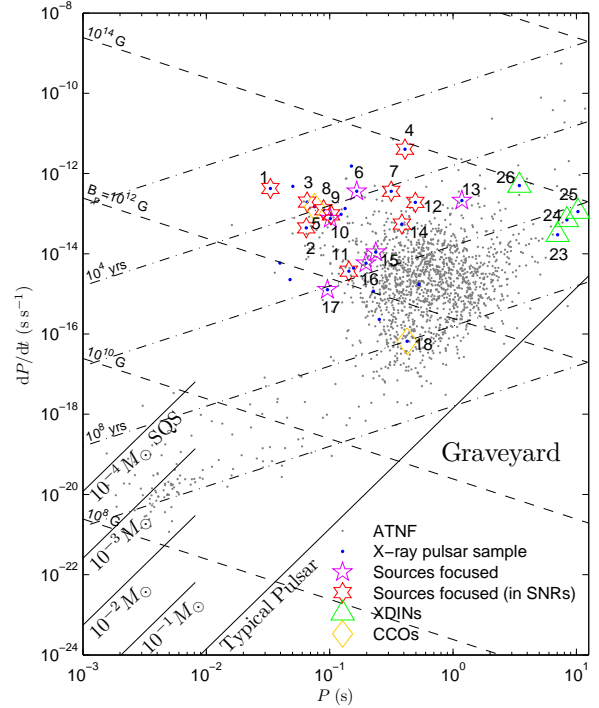

Figure 2. $P - \dot{P}$ diagram for the X-ray pulsar sample. The solid lines are the death lines both for a typical pulsar (with mass of $1.4M_\odot$ and a radius of 10 km) and for low-mass SQSs (with mass of $10^{-4} - 10^{-1}M_\odot$). The hexagonal indicate the focused sources associated with detectable supernova remnants (SNRs), while the pentagons indicate those which exhibit without evident SNRs. The triangles, however, indicate 4 XDINs with measurable temporal parameters, and the diamonds mark the CCOs. The timing parameters for RX J0822-4300 are from Zavlin, Trümper & Pavlov (1999), while the rest are from ATNF Pulsar Catalog[1] .

the energetic Crab pulsar is much likely to be overwhelmed by the nonthermal component originating from its luminous plerion, which hampers the detection to the stellar surface thermal radiation. As an estimate, we, however, adopt a 2σ upper limit to Crab's surface temperature and an inferred radius with assuming a 2 kpc distance between Crab and the earth (Weisskopf et al. 2004). RX J0822-4300, the central stellar remnant in Puppis A, used to be analyzed by Zavlin, Trümper & Pavlov (1999) basing on the *ROSAT* observations in 1990s. They could not confirm whether the X-ray structures surrounding the star belong to the supernova remnant (SNR) or are induced by the probable active magnetosphere. Recent observations on it by *Chandra* and *XMM-Newton* telescopes, however, did not reveal the presence of the associated plerion, indicating an inert magnetosphere (Hui & Becker 2006). Because of the ambiguity of this source, we temporarily make it as one of the active source candidates.

Furthermore, we emphasize these X-ray sources that own measurable spin parameters in the $P - \dot{P}$ diagram (Fig. 2), by which a distribution of them can be read. Other 10 X-ray sources with constraints on the upper limits of their bolometric luminosity are also denoted in the

No.	Source	t (kyr)	$T_{s,1}^{\infty}$ (MK)	R_1^{∞} (km)	$T_{s,2}^{\infty}$ (MK)	R_2^{∞} (km)	L_{bol}^{∞} (10^{33} ergs s^{-1})	Refs.
1	PSR B0531+21 (Crab)	1	$\lesssim 1.85$	$\gtrsim 15$	–	–	~ 18.8	(1)
2	PSR J1811-1925 (in G11.2-0.3)	2	$\leqslant 1.74$	–	–	–	–	(2)
3	PSR J0205+6449 (in 3C 58)	0.82-5.4	≈ 1.7	≈ 2.6	–	–	≈ 0.44	(3)
4	PSR J1119-6127 (in G292.2-0.5)	~ 1.6	$2.4_{-0.2}^{+0.3}$	$3.4_{-0.3}^{+1.8}$	–	–	$2.0_{-0.4}^{+2.5}$	(4)
5	RX J0822-4300 (in Pup A)	2-5	$2.61_{-0.26}^{+0.30}$	$3.29_{-0.74}^{+1.12}$	$5.04_{-0.20}^{+0.28}$	$0.75_{-0.15}^{+0.12}$	≈ 6.2	(5)
6	PSR J1357-6429	~ 7.3	1.7 ± 0.2	2.5 ± 0.5	–	–	≈ 0.37	(6)
7	RX J0007.0+7303 (in CTA 1)	10-30	< 0.66	≈ 12	–	–	$< 4.0 \times 10^{-2}$	(7)
8	PSR B0833-45 (Vela)	11-25	1.06 ± 0.03	$5.1_{-0.3}^{+0.4}$	$2.16_{-0.07}^{+0.06}$	$0.73_{-0.07}^{+0.09}$	$0.31_{-0.04}^{+0.05}$	(8)
9	PSR B1706-44 (in G343.1-02.3)	~ 17	$2.01_{-0.20}^{+0.18}$	$1.81_{-0.29}^{+0.43}$	–	–	≈ 0.38	(9)
10	PSR B1823-13	~ 21	$1.61_{-0.07}^{+0.10}$	~ 2.5	–	–	≈ 0.30	(10)
11	PSR J0538+2817 (in S147)	30 ± 4	$2.12_{-0.03}^{+0.04}$	1.68 ± 0.05	–	–	≈ 0.46	(11)
12	PSR B2334+61 (in G114.3+0.3)	~ 41	1.62 ± 0.23	$1.66_{-0.39}^{+0.59}$	–	–	≈ 0.11	(12)
13	PSR B1916+14	~ 88	$1.5_{-0.6}^{+1.1}$	$0.8_{+5.2}^{-0.6}$	–	–	≈ 0.03	(13)
14	PSR B0656+14 (in Monogem Ring)	~ 110	0.91 ± 0.05	≈ 14	1.9 ± 0.4	≈ 0.8	≈ 0.96	(14)
15	PSR J0633+1746 (Geminga)	~ 340	0.5 ± 0.01	8.6 ± 1.0	1.9 ± 0.3	0.04 ± 0.01	$\approx 3.2 \times 10^{-2}$	(15)
15′			0.482	≈ 10	–	–		(15′)
16	PSR B1055-52	~ 540	0.79 ± 0.03	$12.3_{-0.7}^{+1.5}$	1.79 ± 0.06	0.46 ± 0.06	≈ 0.46	(15)
17	PSR J2043+2740	~ 1200	≈ 0.9	≈ 2	–	–	$\approx 2.0 \times 10^{-2}$	(16)
18	1E 1207.4-5209 (in PKS 1209-51/52)	$\sim 7_{-4}^{+13}$	1.90 ± 0.01	4.5 ± 0.1	3.70 ± 0.02	0.83 ± 0.02	≈ 2.1	(17,18)
19	CXOU J232327.9 +584842 (in Cas A)	0.3	6.14 ± 0.46	$0.41_{-0.07}^{+0.08}$	–	–	$1.7_{-0.9}^{+1.6}$	(19)
20	CXOU J085201.4 -461753 (in G266.2-1.2)	< 1.1	4.68 ± 0.06	0.28 ± 0.01	–	–	0.25 ± 0.02	(20)
21	PSR J1852+0040 (in Kes 79)	–	5.10 ± 3.48	0.9 ± 0.2	–	–	3.7 ± 0.9	(21)
22	PSR J1713-3949 (in G347.3-0.5)	–	4.4	2.4	–	–	15	(22)
23	RX J1856.5-3754	~ 500	≈ 0.74	5.0	–	–	$\approx 5.2 \times 10^{-2}$	(23)
24	RX J0720.4-3125	~ 1300	≈ 0.94	≈ 6.1	–	–	≈ 0.21	(24)
25	RBS 1223^a	~ 400	1.04	0.8	–	–	5.1×10^{-3}	(25)
26	RX J0420.0-5022	~ 110	$0.66_{-0.54}^{+0.29}$	1.4	–	–	2.7×10^{-3}	(26)
27	RX J0806.4-4123	–	1.09 ± 0.01	≈ 0.6	–	–	$\approx 3.6 \times 10^{-3}$	(27)
28	RX J1605.3+3249	–	1.07	≈ 1.1	–	–	1.1×10^{-2}	(25)
29	RBS 1774^b	–	1.04	≈ 1.1	–	–	1.1×10^{-2}	(25)

^{a} 1RXS J130848.6+212708
^{b} 1RXS J214303.7+065419

Table 1. Observational parameters on X-ray sources, including the surface temperature components $T_{s,1/2}^{\infty}$, the emission size components $R_{1/2}^{\infty}$ and the bolometric X-ray luminosity L_{bol}^{∞}. These are the values detected nearby the earth and fitted or analyzed by the black body model. Noting that (i) the age of 1E 1207.4-5209 (source No. 18) is adopted according to the estimate of the associated SNR, which is given by the reference (17); (ii) the ages of RBS 1223 and RX J0420.0-5022 are assessed by spindown ages in this work; (iii) the age limits of sources No. 1, 3-9, 11-12, 14-17, 23-24 are from Yakovlev et al. (2008), while the rest ages are from the corresponding literatures listed in the last column; (iv) for 5 XDINs (No. 25 to 29), the black body parameters are obtained with an assumed distance of 100 pc, as a result of the lack or uncertain of their distances; (v) the spectral parameters for these sources are from the references listed in the last column: (1) Weisskopf et al. (2004) (2) Zhu et al. (2009) (3) Slane et al. (2004a) (4) Gonzalez et al. (2005) (5) Hui & Becker (2006) (6) Zavlin (2007a) (7) Halpern et al. (2004) (8) Manzali, De Luca & Caraveo (2007) (9) McGowan et al. (2004) (10) Pavlov, Kargaltsev & Brisken (2008) (11) McGowan et al. (2003) (12) McGowan et al. (2006) (13) Zhu et al. (2009) (14) Possenti, Mereghetti & Colpi (1996) (15) De Luca et al. (2005) (15′) Jackson & Halpern (2005) (16) Zavlin & Pavlov (2004) (17) Pavlov et al. (2002) (18) De Luca et al. (2004) (19) Chakrabarty et al. (2001) (20) Kargaltsev et al. (2002) (21) Gotthelf, Halpern & Seward (2005) (22) Pavlov, Sanwal & Teter (2004) (23) Ho et al. (2007) (24) Kaplan et al. (2003) (25) Haberl (2004) (26) Haberl, Pietsch & Motch (1999) (27) Haberl & Zavlin (2002).

diagram (Becker & Aschenbach 2002). Besides the death line for a typical pulsar, those for low-mass SQSs are also drawn in the diagram. These death lines set boundaries of the "graveyard" for pulsars with different mass. The timing parameters are from ATNF Pulsar Catalog[1] (Manchester et al. 2005), except for RX J0822-4300, which refers to Zavlin, Trümper & Pavlov (1999).

For magnetosphere-active pulsar candidates, SQSs could suggest themselves to reproduce the cooling processes, while, for magnetosphere-inactive pulsar candidates, possible approaches to understand their current X-ray luminosities could also be proposed by SQSs. These two will be presented in §3.1 and §3.2.

3.1 Cooling of active pulsar candidates

If two isotropic black body emission components—the hot component for polar caps and the warm one for the bulk of the star—are defined for SQSs, then the equation describing cooling processes could be written as (cf. equation (1))

$$L_{\rm SH} = 4\pi R^2 \sigma T_{\rm s}^4 + 4\pi r_{\rm p}^2 \sigma T_{\rm p}^4, \tag{11}$$

and the relation between $T_{\rm s}$ and $T_{\rm p}$ is given by equation (6). The luminosity of stellar heating, $L_{\rm SH}$, could either follow the 1/2-law or the linear-law (see Appendix A). Cooling behavior could thus be calculated by assuming SQSs rotate as orthogonal rotators and slow down as a result of magnetic dipole radiation with magnetic field strength at the poles of 10^{12} G. We provide a parameter space to fit the observational temperature-age data, and the comparison between the observations and expectations are shown in Figs. 3 (for 1/2-law case) and 4 (for linear-law case). Some pulsars demonstrate two black body components in their thermal spectra, e.g. Vela pulsar and the Three Musketeers, implying that the temperature inhomogeneity on these pulsars could be significant. We thus carried out a temperature-difference fit at the same time, as have been shown in the *right* panels in both Figs. 3 and 4. It is worth of noting that, for Geminga, if the photon index of the power-law (PL) component is thawed when fitting its phase-resolved spectra, the entry of the hot black body component could not improve the fits remarkably, or it may even becomes an artifact. This may mean the fluctuation of the magnetospheric emission during a spin cycle might mislead the understanding on its X-ray spectra, as analyzed by Jackson & Halpern (2005) and their results are denoted by No. 15′ in Table 1. If this situation holds, the surface temperature fluctuation on Geminga could be tiny so that undetectable. We, hence, set a rough upper limit to the temperature difference for Geminga of an order lower than its surface temperature, as denoted by 15′ in the "temperature difference-age" figures.

The proposed relation between the rotational kinetic energy loss rate and the bolometric luminosity could inversely provide direct measurement to the moments of inertia of the active X-ray sources. The results are exhibited in Table 2 and could be understood in the SQSs' regime, especially low-mass ones (cf. the adoption of the coefficients C and η in Figs. 3 and 4). We note that for SQSs with $0.01{\rm M}_\odot$, $0.1{\rm M}_\odot$, $1.0{\rm M}_\odot$ and $2.0{\rm M}_\odot$, the moments of inertia I_{45} (i.e. moments

---

[1] www.atnf.csiro.au/research/pulsar/psrcat.

Mass	$\frac{\dot{M}}{\mu}(10^{-9}$ M$_\odot$ yr^{-1})	$\frac{L_{\rm bol}}{\mu \cdot \eta_{\rm acc}}(10^{38}$ ergs s^{-1})
$10^{-4}{\rm M}_\odot$	5.7×10^{-1}	3.5×10^{-2}
$10^{-3}{\rm M}_\odot$	1.2	7.6×10^{-2}
$10^{-2}{\rm M}_\odot$	2.7	1.7×10^{-1}
$10^{-1}{\rm M}_\odot$	5.7	4.7×10^{-1}
$1.0{\rm M}_\odot$	12.4	2.0

Table 4. The bolometric X-ray luminosity ($L_{\rm bol}$) contributed by a SQS's accretion in the *propeller* regime. The corresponding accretion rates, $\dot{M}$, are also given. Noting that the values of luminosities are calculated by adopting $\Delta\varepsilon$, the latent heat per baryon during the phase transition, equals 100 MeV.

of inertia scaled by 10^{45} g cm^2) are $\sim 2.55 \times 10^{-4}$, ~ 0.01, ~ 0.55 and ~ 1.74 respectively.

3.2 Thermal X-ray emission of inactive pulsar candidates

As has been discussed in §2.3.2, one probable energy source to be responsible for the soft X-ray emission of magnetosphere-inactive pulsar candidates lies in the accretion in the *propeller* regime. The accretion could be either to the interstellar medium or to the fallback disk. Numerical results for relevant parameters related to this scenario will be presented here. Equation (1) for this case could be specified as

$$L_{\rm bol} = \frac{GM \cdot \eta_{\rm acc} \cdot \dot{M}}{R} + \Delta\varepsilon \frac{\eta_{\rm acc} \cdot \dot{M}}{m_{\rm p}}, \tag{12}$$

with considering equation (10) and the stellar residual thermal energy is too small to be taken into account. Table 3 exhibits the parameters for the sources under the scenario of accretion in the propeller regime. These parameters include the light cylinder radius $r_{\rm L}$, the corotation radius $r_{\rm co}$, and the Alfvén radius $r_{\rm m}$. Table 4 lists the luminosities of SQSs under the accretion scenario. It could be concluded that the sources' current observational thermal X-ray luminosities could be interpreted by considering the parameters μ, the accretion rate in unit of that of Eddington, and $\eta_{\rm acc}$, the accretion efficiency, e.g. $\mu = 0.01$, $\eta_{\rm acc} = 0.001$. Noting that for the enigmatic central stellar remnant, RX J0822-4300, we also present its results in this case, since we could not exclude the possibility that the star's bolometric luminosity is of accretion origin.

4   CONCLUSIONS AND DISCUSSIONS

We collate the thermal observations of 29 X-ray isolated pulsars and, in the SQSs' regime, for the magnetospherically active pulsar candidates, establish their cooling processes (Figs. 3 and 4), while for the magnetospherically inactive or dead pulsar candidates, interpret the X-ray luminosities under the accretion scenario (Tables 3 and 4). SQSs, because of the possibility of being low-mass, could provide an approach to understand the small black body emission sizes. We note
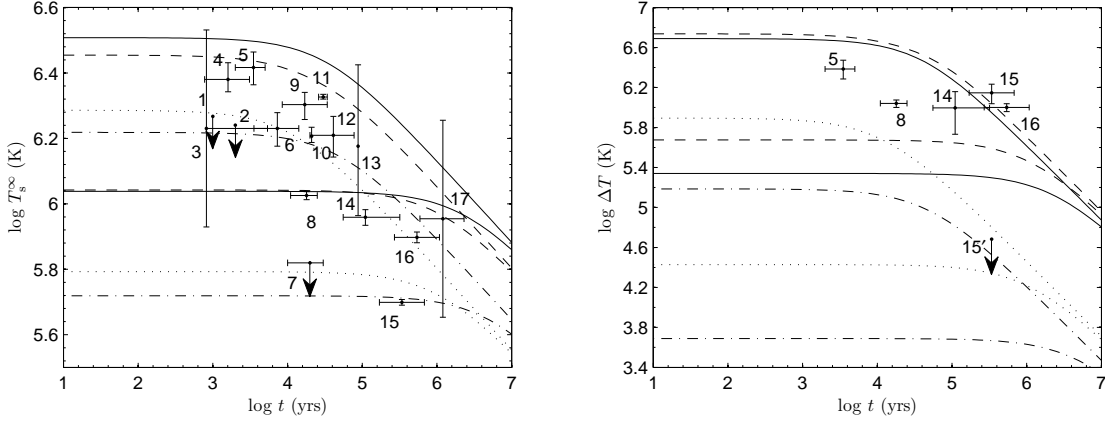
Figure 3. *Left* panel: Cooling curves for SQSs, if the 1/2-law between the bolometric luminosity and the spin energy loss rate holds. *Right* panel: Corresponding temperature differences between the hot and warm components of SQSs, or $\Delta T = T_{\mathrm{p}}^{\infty} - T_{\mathrm{s}}^{\infty}$. The parameters in both panels: $M = 0.1 \mathrm{M_{\odot}}$, $C = 10^{16}$ (solid lines); $M = 1.0 \mathrm{M_{\odot}}$, $C = 10^{16}$ (dashed lines); $M = 1.0 \mathrm{M_{\odot}}$, $C = 10^{15}$ (dotted lines); $M = 0.01 \mathrm{M_{\odot}}$, $C = 10^{15}$ (dash-dot lines) (C is in unit of $\mathrm{ergs}^{1/2}\ \mathrm{s}^{-1/2}$). For two curves with same M and C, the upper one corresponds to an initial spin of 10 ms, while the lower one 100 ms. Noting that the errors on the surface temperatures of PSRs J0205+6449 (No. 3) and J2043+2740 (No. 17) are not provided by the authors of the references, we then conservatively adopt them as deviating from the central values by a factor of 2.
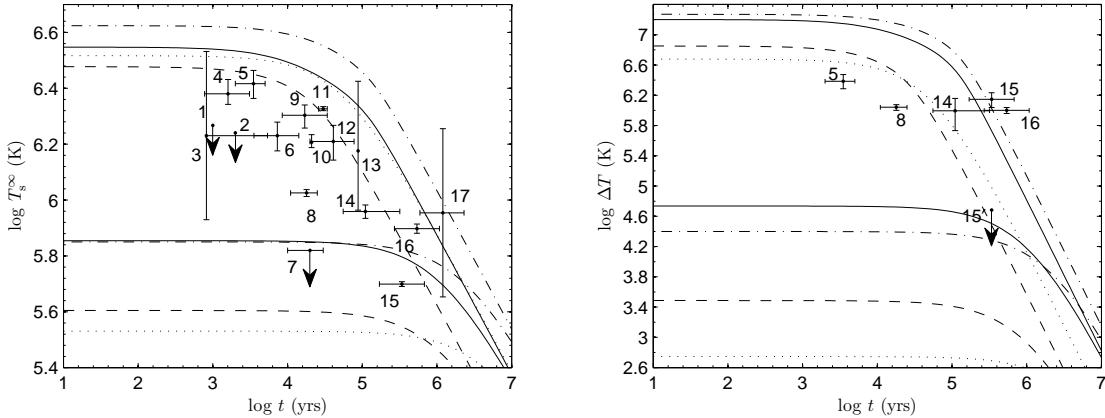

Figure 4. *Left* panel: Cooling curves for SQSs, if the linear-law holds. *Right* panel: Temperature differences for this case. The parameters: $M = 1.0 \mathrm{M_{\odot}}$, $\eta = 0.01$ (solid lines); $M = 1.0 \mathrm{M_{\odot}}$, $\eta = 0.001$ (dashed lines); $M = 0.1 \mathrm{M_{\odot}}$, $\eta = 0.1$ (dash-dot lines); $M = 0.01 \mathrm{M_{\odot}}$, $\eta = 0.1$ (dotted lines). As in Fig. 3, for two curves with same M and η, the upper one corresponds to an initial spin of 10 ms, while the lower one 100 ms.

that for SQSs with mass of $0.01 \mathrm{M_{\odot}}$, $0.1 \mathrm{M_{\odot}}$ and $1 \mathrm{M_{\odot}}$, their radii are ~ 1.8, ~ 3.8 and ~ 8.3 km respectively. On the other hand, a linkage between the pulsars' rates of rotational kinetic energy loss and the bolometric X-ray luminosities is explored by SQSs (see Appendix A), and Table 2 exhibits the evaluated moments of inertia. We hence conclude that SQSs could not be ruled out by the observations on the X-ray isolated pulsars. Additionally, the various performances of X-ray pulsars may indicate their current states or properties and imply their possible evolutionary history. We thus extend a discussion below.

4.1 Spin-powered pulsars

Spin has always been a significant energy source for active pulsars, by which multiwave bands' nonthermal radiation are driven, including those both of the pulsars' and the surrounding plerions'. Some phenomenological studies demonstrate certain regularities for such a population. A brief summary is that the nonthermal X-ray luminosity and spin energy loss rate own a relation of $L_{\mathrm{X}} = 10^{-3} \dot{E}$ (Becker & Trümper 1997), and the γ-ray luminosity is proportional to the square root of $\dot{E}$ or $L_{\gamma} \propto \dot{E}^{1/2}$ (Thompson 1997). We, additionally, note that $V \propto \dot{E}^{1/2}$, where V is the potential drop along the open field region. Therefore, it seems that for such a population the more younger the larger $\dot{E}$ and V that a pulsar owns (cf. Fig. A1, *bottom* panel) and the more luminous of the radiation in the hard X-ray and γ-ray bands.

Besides nonthermal emission, spin may also be an energy origin of pulsars' thermal radiation as the relations of $L_{\mathrm{bol}}^{\infty} \propto \dot{E}^{1/2}$ or $L_{\mathrm{bol}}^{\infty} \sim 10^{-3} \dot{E}$ could exist observationally (see Appendix A for details). SQSs predominantly follow

No.	Source	ν (s^{-1})	$\dot{\nu}$ (s^{-2})	$I_{45}^a \cdot C^2$ (ergs s^{-1})	$I_{45} \cdot \eta$
1	PSR B0531+21 (Crab)	30.225437	-3.862×10^{-10}	7.7×10^{29}	4.1×10^{-5}
2	PSR J1811-1925	15.463838	-1.052×10^{-11}	–	–
3	PSR J0205+6449	15.223856	-4.495×10^{-11}	5.8×10^{28}	4.6×10^{-5}
4	PSR J1119-6127	2.452508	-2.419×10^{-11}	1.7×10^{30}	8.5×10^{-4}
5	RX J0822-4300	13.2856716499(3)	$-2.6317(3)\times10^{-11}$	2.7×10^{30}	2.8×10^{-4}
6	PSR J1357-6429	6.020168	-1.305×10^{-11}	4.4×10^{28}	1.2×10^{-4}
7	RX J0007.0+7303	3.165922	-3.623×10^{-12}	3.5×10^{27}	8.8×10^{-5}
8	PSR B0833-45 (Vela)	11.194650	-1.567×10^{-11}	1.4×10^{28}	4.5×10^{-5}
9	PSR B1706-44	9.759978	-8.857×10^{-12}	4.2×10^{28}	1.1×10^{-4}
10	PSR B1823-13	9.855532	-7.291×10^{-12}	3.2×10^{28}	1.1×10^{-4}
11	PSR J0538+2817	6.985276	-1.790×10^{-13}	4.3×10^{30}	9.3×10^{-3}
12	PSR B2334+61	2.018977	-7.816×10^{-13}	1.8×10^{29}	1.7×10^{-3}
13	PSR B1916+14	0.846723	-1.523×10^{-13}	1.8×10^{29}	5.9×10^{-3}
14	PSR B0656+14	2.598137	-3.713×10^{-13}	1.1×10^{31}	1.7×10^{-2}
15	PSR J0633+1746 (Geminga)	4.217640	-1.952×10^{-13}	3.2×10^{28}	9.9×10^{-4}
16	PSR B1055-52	5.073371	-1.501×10^{-13}	6.9×10^{30}	1.5×10^{-2}
17	PSR J2043+2740	10.402519	-1.374×10^{-13}	7.1×10^{27}	3.5×10^{-4}

^{a} $I_{45} = I/(10^{45}$ g cm^2)

Table 2. The moments of inertia of active pulsar candidates suggested by SQSs. The 5th column lists the values derived by the 1/2-law, while the 6th column lists those obtained by the linear-law. The temporal parameters are from ATNF Pulsar Catalog (see footnote 1 for the website). For RX J0822-4300, we note that we adopt the spin parameters obtained by Zavlin, Trümper & Pavlov (1999) basing on a 4.5 yr-span data set, though Hui & Becker (2006) provided more recent values using a 0.5 yr-span data set.

these relations to accomplish their cooling processes, since their residual thermal energy could be quite inadequate to sustain a long term X-ray thermal emission. This could be the different nature when comparing with neutron stars, whose cooling is powered by residual thermal energy.

Furthermore, it could be an intrinsic distinction for SQSs from neutron stars that the heat capacity of SQSs is much lower than that of neutron stars. The thermal X-ray emission of SQSs could only be sustained by heating, and the missing compact object in SN1987A (McCray 2007) could be a SQS with negligible residual thermal energy and thus is not X-ray loud observationally.

4.2 Accretion-powered pulsars

XDINs and CCOs could be representative populations of magnetosphere-inactive pulsars. Nevertheless, their energy origin that could power the X-ray emission is still an enigma. The bolometric luminosities of 1E 1207.4-5209, RX J1856.5-3754 and RX J0720.4-3125 exceed their spin energy loss rates by a factor of ~ 60, ~ 15 and ~ 45, respectively; they do not appear to be powered by spin.

CCOs could be a group of weakly-magnetized and long-initial-period pulsars (Pavlov et al. 2002; Gotthelf & Halpern 2007), because of which the potential drop along the open field lines could be much less than $\sim 10^{12}$ V, so that the primary plasma could not be fully accelerated and result in an inactive magnetosphere. The black body fits to the thermal spectra of CCOs always result in extremely small emission sizes (Pavlov, Sanwal & Teter 2004), implying possible existence of low-mass SQSs, even as low as $\sim 10^{-4}\mathrm{M}_\odot$ (Xu 2005). Hence, from another perspective, CCOs' $\dot{E}$ might be very low, so that effective

magnetospheric emission and plerions could not be driven. CCOs could thus be the representatives of a group of natal inactive pulsars. Accretion to the fallback ejecta of the associated SNRs could power their soft X-ray luminosity, and this scenario have been mentioned by several authors (e.g., Chakrabarty et al. 2001; Kargaltsev et al. 2002; Fesen, Pavlov & Sanwal 2006; Halpern et al. 2007).

XDINs, owning comparatively larger spindown ages and stronger magnetic fields, might be the descendants of magnetars. Considering similar properties between them (Haberl 2004; Mereghetti 2008), one could not exclude that XDINs are still being powered by the decaying magnetic fields. However, observations have revealed the probable existence of residual disks around such pulsars, and thus their radiation may be of accretion origin (Lo Curto et al. 2007). In this case, XDINs could be the evolved products of active pulsars, and thanks to the accretion so that they are still visible after their death. Most XDINs have absorption features in their spectra, being similar to those of CCOs. Hence, if they are really undergoing accretion in the propeller regime, their spindown rates, $\dot{P}$, could then be of accretion origin rather than causing by the magnetic dipole braking. Thus their magnetic fields could be much lower than the values determined by canonical magnetic dipole radiation, since the absorption features could be electron cyclotron lines. Therefore, the common properties of absorption features between XDINs and CCOs could imply that XDINs might be older CCOs. XDINs and CCOs have not manifested themselves as radio pulsars, their radio-quiet demonstrations could be an intrinsic property rather than being of beaming origin, since they might be dead or natal inactive ones. So they could be grouped as radio-quiescent pulsars. For RX J0007.0+7303, an active pulsar candidate, its lack of

No.	Source	ν (s^{-1})	$\dot{\nu}$ (s^{-2})	$r_{\rm L}(10^{10}$ cm)	$r_{\rm co}(10^8$ cm)	$r_{\rm m}\cdot\mu^{2/7}(10^8$ cm)
5	RX J0822-4300	13.2856716499(3)	-2.6317(3)$\times10^{-11}$	3.59$\times10^{-2}$	1.24$\times10^{-2}$	5.05$\times10^{-1}$
					2.67$\times10^{-2}$	8.74$\times10^{-1}$
					5.76$\times10^{-2}$	1.51
					1.24$\times10^{-1}$	2.62
					2.67$\times10^{-1}$	4.53
18	1E 1207.4-5209	2.357764	$(-3.669\pm5.1)\times10^{-16}$	0.20	0.18	0.27
					0.39	0.47
					0.85	0.82
19	CXOU J232327.9+584842	–	–	–	–	–
20	CXOU J085201.4-461753	–	–	–	–	–
21	PSR J1852+0040	9.531742	$(3.089\pm2.5)\times10^{-14}$	–	–	–
22	PSR J1713-3949	2.548086	–	–	–	–
23	RX J1856.5-3754	0.141739	-5.980×10^{-16}	3.37	1.19	3.49
					2.56	6.04
					5.52	10.46
24	RX J0720.4-3125	0.119174	-9.918×10^{-16}	4.00	1.33	4.68
					2.88	8.10
					6.20	14.02
25	RBS 1223	0.096969	-1.053×10^{-15}	4.92	1.53	4.97
					3.30	8.59
					7.11	14.86
26	RX J0420.0-5022	0.289597	-4.193×10^{-14}	1.65	0.74	6.38
			$\pm8.0\times10^{-13}$		1.59	11.03
					3.43	19.08
27	RX J0806.4-4123	0.087943	$(3.558\pm5.0)\times10^{-14}$	–	–	–
28	RX J1605.3+3249	0.1453?	–	–	–	–
29	RBS 1774	0.105966	–	–	–	–

Table 3. Numerical values of the parameters under the *propeller* regime if the sources own detectable spindown parameters. The parameters include the light cylinder radius $r_{\rm L}$, the corotation radius $r_{\rm co}$, and the Alfvén or the magnetosphere radius $r_{\rm m}$. For each source, three values on $r_{\rm co}$ and $r_{\rm m}$ are given, which, from top to bottom, correspond to the results of a 0.01M$_\odot$/0.1M$_\odot$/1.0M$_\odot$-SQS respectively, but the results of RX J0822-4300 are presented more detailed starting from the case of a 10^{-4}M$_\odot$-SQS. The temporal parameters for RX J1605.4-4123 and RX J0822-4300 refer to Haberl (2004) and Zavlin, Trümper & Pavlov (1999) respectively, while those of the rest are from ATNF Pulsar Catalog (see footnote 1 for the website), and we note the errors when they are significant enough.

radio signal could be the result of an unfavorable geometry, or its radio beam sweeps away from the earth as has been analyzed by Brazier & Johnston (1999).

The similar thermal manifestations of accreting pulsars (e.g. XDINs and CCOs) and cooling pulsars may have caused a confusion about distinguishing between the two classes (Treves et al. 2000). However, the activeness of the magnetosphere could provide a way to achieve an identification. If pulsars are in fact SQSs with rapid rotation, cooling pulsars are then likely to be undergoing the spindown-powered heating evolution, and multi-bands non-thermal emission originating from luminous magnetospheres and even PWNe will accompany such coolers during the processes. In contrast, accreting pulsars may have not demonstrate such characteristics observationally. In this context, the CCO in the SNR Cassiopeia A (source No. 19 in Table 1) should be an accretor because of the lack of PWN and nonthermal power-law component (Pavlov & Luna 2009).

APPENDIX A: SPIN-POWERED THERMAL EMISSION?

In the solid quark star regime, magnetosphere-active pulsars' cooling depends predominantly on the stellar heating as a result of the lack of sufficient residual heat as has been analyzed in §2. The pulsar activity induced stellar heating would have intrinsically set up a linkage between the X-ray bolometric luminosity and the spin energy loss. We, hence, present here a phenomenological study on such a relation.

The sample of active pulsars firstly includes the top 17 sources listed in Table 1. Becker & Aschenbach (2002) summarized X-ray pulsars, in which other 10 sources' upper limits on the bolometric luminosities could be defined. These 10 pulsars are meanwhile considered. Fig. A1 (*top* panel) illustrates these sources' bolometric luminosities $L_{\rm bol}^\infty$ as a function of their spin energy loss rates $\dot{E}$, and Table A1 lists the fitted parameters led by the function of

$$\log L_{\rm bol}^\infty = p1\cdot\log\dot{E} + p2. \tag{A1}$$

The fits are carried out both only for the top 17 pulsars taken from Table 1 (as Group A) and for the whole sample with the other 10 sources included at the same time(as Group B). The best fits, moderate clearly, suggest a 1/2-law on the

Group	$p1^a$	$p2$	Corr. Coef.^{b}	χ_r^2 (d.o.f)^c
A.	0.4561 ± 0.2315	16.20 ± 8.30	–	$0.3277(14)$
	(1)	$-3.280^{+0.495}_{-0.494}$	0.7487	$0.8607(15)$
B.	$0.5918^{+0.2045}_{-0.2046}$	$11.66^{+7.3100}_{-7.2990}$	–	$0.6081(24)$
	(1)	-2.896 ± 0.403	0.7730	$0.9964(25)$

^{a} Values in the parenthesis are frozen during the fits. The errors are in 95% confidence level.
^{b} Correlation coefficient of the data between bolometric luminosity and $\dot{E}$.
^{c} Reduced χ^2, or χ^2 per degree of freedom (d.o.f).

Table A1. Fitting parameters for $L_{\rm bol}^\infty$—$\dot{E}$ data, which has been shown in Fig. A1 (*top* panel).

relation between pulsars' bolometric luminosities and the spin energy loss rates, or

$$L_{\rm bol}^\infty(\dot{E}) = C\dot{E}^{1/2}, \tag{A2}$$

with a coefficient $C = 10^{p2}$ in unit of ergs$^{1/2}$ s$^{-1/2}$. If $p1$ is fixed at 1, a linear-law then is implied, i.e.

$$L_{\rm bol}^\infty(\dot{E}) = \eta \cdot \dot{E}, \tag{A3}$$

with a coefficient $\eta = 10^{p2}$, or, in other words, η is the conversion efficiency. The fits obtain $\eta \sim 10^{-3}$, which is similar to the nonthermal X-ray case (Becker & Trümper 1997). For the 1/2-law case, the conversion efficiency turns out to be the function of $\dot{E}$, and it could be

$$\eta(\dot{E}) = \frac{C\dot{E}^{1/2}}{\dot{E}} = \frac{C}{\dot{E}^{1/2}}, \tag{A4}$$

which could in turn, besides the fits, provide a reference to the value of the coefficient C by a natural constraint of $\eta(\dot{E}) < 1$. Taking B0823+26, the minimum $\dot{E}$ in our sample, as an example, its C could be less than $\sim \sqrt{10^{32}} = 10^{16}$ ergs$^{1/2}$ s$^{-1/2}$. Additionally, we note here that we also present a age-$\dot{E}$ relation in the *bottom* panel of Fig. A1, which illustrates a natural trend for spin-powered pulsars.

ACKNOWLEDGEMENT

REFERENCES

Alcock C., Farhi E., Olinto A., 1986, ApJ, 310, 216
Alford M. G., Rajagopal K., Schaefer T., Schmitt A., 2008, Rev. Mod. Phys. in press (arXiv:0709.4635)
Arons J. 1981, ApJ, 248, 1099

Becker W., Aschenbach B., 2002, in WE-Heraeus Seminar on Neutron Stars, Pulsars and Supernova Remnants, Eds. W. Becker, H. Lesch & J. Trümper, Bad Honnef, pp.64
Becker W., Trümper J., 1997, A&A, 326, 682
Brazier K. T. S., Johnston S., 1999, MNRAS, 305, 671
Chakrabarty D., Pivovaroff M. J., Hernquist L. E., Heyl J. S., Narayan R., 2001, ApJ, 548, 800
Cheng A. F., Ruderman M. A., 1977, ApJ, 214, 598
De Luca A., Mereghetti S., Caraveo P. A., Moroni M., Mignani R. P., Bignami G. F., 2004, A&A, 418, 625
De Luca A., Caraveo P. A., Mereghetti S., Negroni M., Bignami G. F., 2005, ApJ, 623, 1051
Fesen R. A., Pavlov G. G., Sanwal D., 2006, ApJ, 636, 848
Flowers E., Itoh N., 1981, ApJ, 250, 750
Gonzalez M. E., Kaspi V. M., Camilo F., Gaensler B. M., Pivovaroff M. J., 2005, ApJ, 630, 489
Gudmundsson E. H., Pethick C. J., Epstein R. I., 1983, ApJ, 272, 286
Gotthelf E. V., Halpern J. P., 2007, ApJ, 664, L35
Gotthelf E. V., Halpern J. P., Seward F. D., 2005, ApJ, 627, 390
Haberl F., Pietsch W., Motch C., 1999, A&A, 351, L53
Haberl F., Zavlin V. E., 2002, A&A, 391, 571
Haberl F., 2004, Advances in Space Research, 33, 638
Halpern J. P., Gotthelf E. V., Camilo F., Helfand D. J., Ransom S. M., 2004, ApJ, 612, 398
Halpern J. P., Gotthelf E. V., Camilo F., Seward F. D., 2007, ApJ, 665, 1304
Ho W. C. G., Kaplan D. L., Chang P., Van Adelsberg M., Potekhin A. Y., 2007, MNRAS, 375, 821
Horvath J., 2005, Mod. Phys. Lett., A20, 2799
Hui C. Y., Becker W., 2006, A&A, 454, 543
Jackson M. S., Halpern J. P., 2005, ApJ, 633, 1114
Kaplan D. L., Van Kerkwijk M. H., Marshall H. L., Jacoby B. A., Kulkarni S. R., 2003, ApJ, 590, 1008
Kargaltsev O., Pavlov G. G., Sanwal D., Garmire G. P., 2002, ApJ, 580, 1060
Lipunov V. M., 1992, Astrophysics of Neutron Stars, Springer-Verlag, Berlin
Lo Curto G., Mignani R. P., Perna R., Israel G. L., 2007, A&A, 473, 539
Madsen, J., 1999, in Hadrons in Dense Matter and Hadrosynthesis, 162, Springer, Berlin
Manchester R. N., Hobbs G. B., Teoh A., Hobbs M., 2005, AJ, 129, 1993-2006
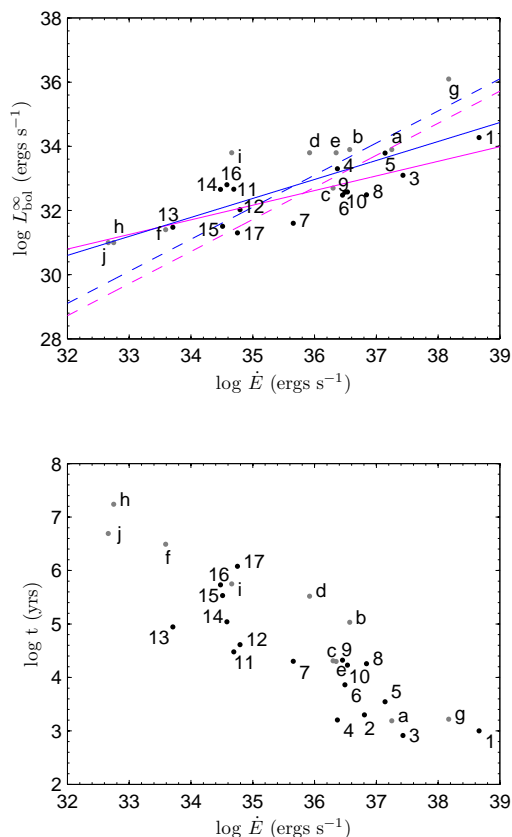Mannarelli, M., Rajagopal, K., Sharma, R. 2007, Phys.

Mereghetti S., 2008, ARAA, 15, 225

Michel F. C., 1988, Phys. Rev. Lett., 60, 677

Owen B. J. 2005, Phys. Rev. Lett., 95, 211101

Pavlov G. G., Luna G. J. M., 2009, ApJ, 703, 910

Pavlov G. G., Sanwal D., Teter M. A., 2004, in: *Young Neutron Stars and Their Environments*, IAU Symp. 218, Eds. F. Camilo & B. M. Gaensler, San Francisco (arXiv:0311526v1)

Pavlov G. G., Zavlin V. E., Sanwal D., Trümper, J., 2002, ApJ, 569, L95

Pavlov G. G., Kargaltsev O., Brisken W. F., 2008, ApJ, 675, 683

Possenti A., Mereghetti S., Colpi M., 1996, A&A, 313, 565

Schwope A. D., Hambaryan V., Haberl F., Motch C., 2005, A&A, 441, 597

Shuryak, E. V. 2009, Prog. Part. & Nucl. Phys., 62, 48

Slane, P., Helfand, D. J., Van de Swaluw, E., Murry, S. S., 2004a, ApJ, 616, 403

Thompson D. J., Harding A. K., Hermsen W., Ulmer M. P., 1997, in AIP Conf. Proc. 410, Proc. Fourth Compton Symposium, ed. C. D. Dermer, M. S. Strickman, J. D. Kurfess (New York: AIP), 39

Treves A., Turolla R., Zane S., Colpi M., 2000, PASP, 112, 297

Usov V. V., 2001, ApJ, 550, L179

Vonsovsky S. V., Katsnelson M. I., 1989, Quantum Solid-State Physics, Springer-Verlag, Berlin

Wang F. Y. -H., Ruderman M. A., Halpern J. P., Zhu T., 1998, ApJ, 498, 373

Weisskopf M. C., O'Dell S. L., Paerels F., Elsner R. F., Becker W., Tennant A. F., Swartz D. A., 2004, ApJ, 601, 1050

Xu R. X., 2003, ApJ, 596, L59

Xu R. X., 2005, MNRAS, 356, 359

Xu R. X., 2009, J. Phys. G: Nucl. Part. Phys. 36, 064010

Yakovlev D. G., Haensel P., 2003, A&A, 407, 259

Yakovlev D. G., Pethick C. J., 2004, ARAA, 42, 169

Yakovlev D. G., Gnedin O. Y., Kaminker A. D., Potekhin A. Y., 2008, AIPC, 983, 379

Zavlin V. E., 2007, ApJ, 665, L143

Zavlin V. E., Pavlov G. G., 2004, ApJ, 616, 452

Zavlin V. E., Trümper J., Pavlov G. G., 1999, ApJ, 525, 959

Zhang B., Harding A. K., 2000, ApJ, 532, 1150

Zhang X., Xu R. X., Zhang S. N., 2004, in: *Young Neutron Stars and Their Environments*, IAU Symp. 218, Eds. F. Camilo & B. M. Gaensler, San Francisco, pp.303

Zhu W. W., Kaspi V. M., Gonzalez M. E., Lyne A. G., 2009, ApJ, in press (arXiv:0909.0962v1)

Figure A1. Functions $L_{\rm bol}^{\infty}(\dot{E})$ (*top* panel) and $t(\dot{E})$ (*bottom* panel) of active pulsar candidates. In the *top* panel, the fits are carried out both for Group A (including top 17 pulsars listed in Table 1; they are marked by dark points and their numbers here) and Group B (including the members in Group A and the other 10 sources whose upper limits on the bolometric luminosities could be defined observationally; the 10 sources are marked by grey points and letters). Red lines are the fitted results for Group A, while blue lines are those for Group B. In both groups, solid lines provide the best fit to the data, while the dashed lines give the fits by freezing $p1$ at 1. We note that the 10 sources with upper limits on their bolometric luminosities defined are taken from Becker & Aschenbach (2002), and they are a. B1509-58, b. B1951+32, c. B1046-58, d. B1259-63, e. B1800-21, f. B1929+10, g. B0540-69, h. B0950+08, i. B0355+54, j. B0823+26.

Rev. D76, 4026

Manzali A., De Luca A., Caraveo P. A., 2007, ApJ, 669, 570

McCray R., 2007, in: Supernova 1987A: 20 Years After, eds. S. Immler, K. Weiler, & R. McCray (American Inst. Physics), pp. 3-14

McGowan K. E., Kennea J. A., Zane S., Córdova F. A., Cropper M., Ho C., Sasseen T., Vestrand W. T., 2003, ApJ, 591, 380

McGowan K. E., Zane S., Cropper M., Kennea J. A., Córdova F. A., Ho C., Sasseen T., Vestrand W. T., 2004, ApJ, 600, 343

McGowan K. E., Zane S., Cropper M., Vestrand W. T., Ho C., 2006, ApJ, 639, 377